



Sound generation by entropy inhomogeneities in a thermally choked flow nozzle

Frédéric Olivon ¹², Antoine Chédin¹, Jean-Etienne Durand¹, Aurelien Genot², Estelle Piot²

Abstract

The indirect entropy noise generation in a thermally choked flow nozzle, induced by the convection of 2D circular entropy spots, is investigated. Two configurations are examined: a thermal throat formed by non-uniform volumetric heat addition, and an equivalent isentropic nozzle with a geometric throat. Both are designed to produce the same steady Mach number distribution, in order to isolate the influence of heat addition on the acoustic response. The analysis combines two-dimensional CFD simulations with two asymptotic one-dimensional models: the quasi-steady (QSS) model, adapted for large spots, and the point-mass (PM) inertial model, for small spots. For the geometric-throat case, the CFD results show fair agreement with both the QSS and PM predictions in their respective asymptotic regimes. For the thermal-throat case, the QSS regime is reached for spots larger than 100 throat radius, which is a value lower than that of the geometric configuration. Then, the acoustic response exceeds QSS predictions ($\sim 20\%$), which is certainly due to the invalidity of the assumption of no Mach fluctuations at the throat. In the small-spot limit, the PM model predicts the inertial regime with reasonable accuracy for both configurations, but at different spot radii. The thermal-throat case, however, deviates from the PM prediction, highlighting fundamental differences between heated and isentropic nozzles and the need to extend asymptotic models to non-isentropic base flows.

Keywords: Dual-mode ramjet, Thermal throat, Combustion instabilities, Indirect entropy noise

Nomenclature

Latin

A - Cross-sectional area

 c_p – Isobaric specific heat capacity

 c_v – Isochoric specific heat capacity

e - Specific internal energy

 e_0 - Total specific energy = $e + |\mathbf{u}|^2/2$

L - Nozzle length

M - Mach number

p - Static pressure

 P_v – Volumetric heat source term

q – Heat release per unit mass

r - Specific gas constant = \mathcal{R}/\mathcal{W}

 R_s – Entropy-spot radius

s - Specific entropy

t – Time

T – Static temperature

 \mathbf{u} - Velocity vector = (u, v, w)

x – Longitudinal position

y - Transverse position

 $\dot{\dot{m}}$ – Mass flow rate

 \mathcal{R} – Universal gas constant

 \mathcal{W} - Molar mass of the gas

Greek

 α – Divergence angle

 γ – Heat capacity ratio = c_n/c_v

 ρ – Density

Superscripts

()' - Fluctuating quantity

Subscripts

d - Divergent duct

geo - Geometric nozzle

in - Inlet

PM - Point-mass model

QSS - Quasi-steady model

t - Transition duct

tht - Thermal-throat nozzle

u – Uniform duct

0 - Total quantity

* - Critical throat

() – Steady quantity

¹DMPE, ONERA, Université Paris-Saclay, Palaiseau, 91120, France ²DMPE, ONERA, Université de Toulouse, Toulouse, 31000, France

1. Introduction

Dual-mode ramjets, capable of operating in both subsonic and supersonic combustion regimes, are of interest for a wide range of flight Mach numbers relevant to supersonic and hypersonic air-breathing vehicles [1]. A geometric throat is typically placed at the outlet of a conventional ramjet combustion chamber to enable a smooth transition from subsonic to supersonic flow. However, this configuration is unsuitable for scramjet operation, where the flow remains supersonic upstream of the nozzle.

In contrast, the thermal throat [2, 3], a sonic region formed by the heat release from combustion, requires only a divergent nozzle (fig. 1), allowing a seamless transition between subsonic and supersonic combustion. However, this configuration is highly sensitive to disturbances in the reactive flow, which requires a well-optimized combustion chamber design.

Under specific operating conditions, ramjets, scramjets, and dual-mode ramjets are susceptible to combustion instabilities, which can cause pressure oscillations, flashback, combustion chamber extinction, or severe engine damage [4–11].

The development of a dual-mode ramjet incorporating a thermal throat necessitates an investigation of the coupled acoustic–flame–hydrodynamic mechanisms driving these instabilities. In particular, the role of the thermal throat as an acoustic boundary under critical flow conditions remains poorly understood.

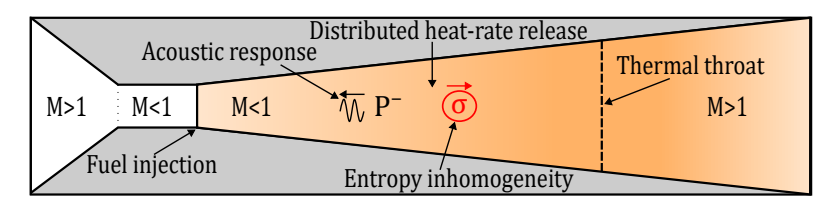


Fig 1. (Color online) Sketch of a simplified dual-mode ramjet incorporating a thermal-throat in the ramjet mode.

The influence of heat addition on flow dynamics has been extensively studied in subsonic regimes, particularly with respect to its impact on acoustic wave propagation. In such flows, the transmission of acoustic waves through a heated medium induces acoustic absorption [12, 13]. Also, acoustic waves can generate entropy waves as they propagate through the heated flow [14–16].

Beyond subsonic regimes in the nozzle, other studies have focused on geometrically choked flows. Particularly, the acoustic response and wave dynamics has been investigated in the geometrically choked flow configuration [17–20]. However, the heat addition as the main contributor to the choking phenomenon is not considered yet, becoming the object of the present work.

In recent contributions [21–23], the acoustic and entropy wave propagation through the thermally choked flow and the obtained aeroacoustic response receives a particular attention. These studies show that the steady heat addition affects significantly the acoustic reflection coefficient at the zero-frequency limit, where it is substantially lower than in geometrically choked configurations. This effect is less pronounced for the entropy-noise production coefficient.

In contrast, the present study aims to investigate the propagation of two-dimensional flow inhomogeneities to analyse indirect combustion noise. Indirect combustion noise, as defined by Morgans and Yang [11], refers to the sound generated by the propagation of flow inhomogeneities, such as vortices, compositional variations, or temperature non-uniformities (also referred to as entropy spots), through a non-uniform base flow. The latter is the focus of this study. Based on the works of Kowalski *et al.* [24] and Elbakly [25] on geometrically choked nozzle configurations, two asymptotic regimes (quasi-steady and inertial) have been identified, corresponding to very large and very small inhomogeneity sizes.

In this study, the aeroacoustic response of a two-dimensional entropy spot is numerically assesses, modeled as a circular two-dimensional disturbance in a thermally choked nozzle flow configuration. A

comparison with an equivalent isentropic nozzle is also conducted to highlight the impact of heat addition on the acoustic response.

2. Methodology

2.1. Simplified dual-mode ramjet geometry and inlet flow conditions

A half-domain planar geometry of a two-dimensional simplified dual-mode ramjet is used to study indirect entropy noise (fig. 2). The nozzle geometry consists of three sections: a straight-duct upstream section ($0 \le x/L < x_{\rm u}/L = 0.42$); a smooth transition section ($x_{\rm u}/L = 0.42 \le x/L < x_{\rm d}/L = 0.58$), formed by a circular-arc wall with angle $\alpha = 3^{\circ}$; and a divergent duct with a constant divergence angle $\alpha = 3^{\circ}$ ($x/L > x_{\rm d}/L = 0.58$).

The total length and inlet height of the nozzle are $L=2.4\,\mathrm{m}$ and $y_{\mathrm{in}}=25\times10^{-3}\,\mathrm{m}$, respectively. The circular arc radius of the transition region is $R_{\mathrm{t}}/y_{\mathrm{in}}=305$. A slip adiabatic boundary condition is imposed on the upper nozzle wall, while a symmetry boundary condition is applied along the lower edge.

Hereafter, the constant cross-sectional duct is referred to as the straight-duct, while the varying cross-sectional region (transition and divergent sections) is referred to as the divergent-duct.

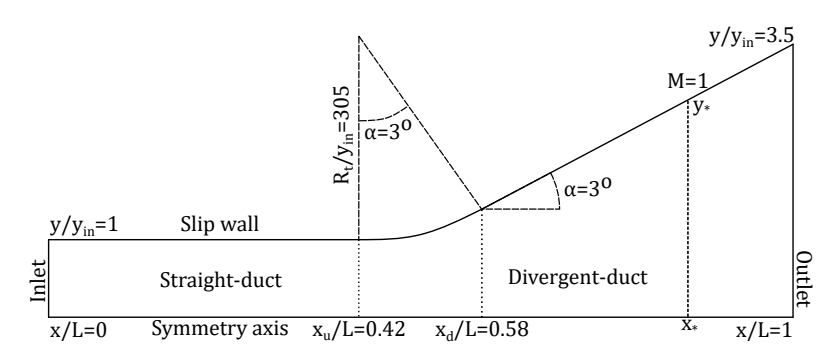


Fig 2. Sketch of the computational domain geometry (not to scale).

The incoming airflow at the inlet is subsonic, as detailed in table 1. The inlet conditions are representative of typical dual-mode ramjet engine operation [2].

Table 1. Nozzle inlet Mach number M_{in} , total temperature $T_{0,in}$, and static pressure p_{in} corresponding to a typical flight Mach number M=3.

Parameter	Value	Unit
Mach number, M _{in}	0.6	-
Total temperature, $T_{0, \text{in}}$	600	K
Static pressure, p_{in}	2	bar

2.2. Flow model and thermodynamic gas properties

For a mono-species gas, assuming no losses due to viscosity or thermal diffusion, and no external force fields, the equations for mass, momentum, and total energy including a volumetric heat source term P_v are considered, as commonly used in the literature [26–28]:

$$\begin{cases}
\frac{\partial \rho}{\partial t} + \nabla \cdot (\rho \mathbf{u}) = 0, \\
\frac{\partial}{\partial t} (\rho \mathbf{u}) + \nabla \cdot (\rho \mathbf{u} \otimes \mathbf{u}) + \nabla p = 0, \\
\frac{\partial}{\partial t} (\rho e_0) + \nabla \cdot [(\rho e_0 + p) \mathbf{u}] = P_v.
\end{cases} \tag{1}$$

A nomenclature is provided detailing all terms. For clarity and conciseness, the system of equations (1) will hereafter be referred to as the Euler equations.

To close the Euler equations (1), the ideal gas law is used:

$$p = \rho r T. (2)$$

Air is modeled as an ideal gas with a specific isobaric heat capacity c_p that varies with temperature. It is computed using a seventh-order polynomial function of the local static temperature T:

$$c_p = \sum_{n=0}^{7} \frac{\alpha_n}{W} T^n, \tag{3}$$

where α_n are the heat capacity coefficients provided by Lemmon *et al.* [29]. For an ideal gas, the specific gas constant can also be expressed as $r = c_p - c_v$.

The impact of boundary layers on thermal throat formation has been investigated by Durand and Olivon [30], who found only a minor influence on thermal throat dynamics. The volumetric heat addition P_v is prescribed as steady, and fluctuations in the heat release are ignored. Following the approach of several authors [3, 12, 17, 21], the feedback loop between the flame and the flow is not considered. As a result, the flow does not influence the heat-release rate. Although this is a strong assumption, as noted by Yeddula *et al.* [31], it enables a proper characterization of the indirect entropy noise behavior.

For a uniform gas composition and a reversible process, the Gibbs energy equation provides a relation between variations in entropy s, temperature T, and pressure p:

$$\frac{\mathrm{d}s}{c_p} = \frac{\mathrm{d}T}{T} - (\gamma - 1)\frac{\mathrm{d}p}{\gamma p}.\tag{4}$$

2.3. Volumetric heat source term model for thermal throat generation

To establish a steady thermal throat deep within the divergent nozzle using a non-uniform heat release, the same approach as in previous works [21, 23, 32, 33] is followed, in which the spatial distribution of P_v is split into two regions. In the straight-duct (fig. 2), the flow is not heated (P_v is set to zero). In the divergent duct ($x > x_u$), the volumetric power distribution P_v follows a log-normal profile in x, as proposed by Wang *et al.* [34].

To adjust $P_v(x)$, a quasi-one-dimensional steady-state model for a calorically semi-perfect ideal gas has been developed, based on the Mach number and static temperature equations formulated by Shapiro [35], along with the steady-state thermal throat condition from Heiser and Pratt [36]. This model does not directly define $P_v(x)$, but instead provides the gradient $\mathrm{d}q/\mathrm{d}x$ of the heat release per unit mass q(x):

$$P_v(x) = \frac{\dot{m}}{\mathsf{A}(x)} \, \frac{\mathsf{d}q}{\mathsf{d}x},\tag{5}$$

where $\dot{m}=\rho u A$ is the quasi-one-dimensional steady mass flow rate through the nozzle cross-sectional area A(x), computed using isentropic relations and the parameters listed in table 1.

The model is tuned to place the steady-state thermal throat at $x_*/L=0.8$, corresponding to a flame length of $(x_*-x_{\rm u})/L=\delta_*/L=0.38$. This location was chosen to match the mean spatial position of the thermal throat observed in *Case C4* of the JAPHAR study by Dessornes and Scherrer [2], in which the feasibility of a thermally choked nozzle was experimentally demonstrated for an incoming H₂ gas mixture at Mach 5. Further details are provided in appendix A.

In what follows, the thermal throat position $()_*$, where the flow is choked, is referred to as the critical throat position. A similar definition applies to the geometric-throat configuration (see section 2.4).

2.4. Geometric throat nozzle geometry for comparison

To compare the aeroacoustic response induced by the propagation of entropy inhomogeneities within a thermally choked flow nozzle, a nozzle with a geometric throat is also considered. This nozzle is constructed using the same spatial Mach number profile, M(x), as that obtained from the thermally choked flow configuration described in section 2.3. The geometry of the isentropic flow nozzle, denoted A_{is} , is determined using the following expression, assuming a constant specific heat ratio γ_{in} :

$$A_{is}(x) = \frac{A_{in}M_{in}}{M_{tht}} \left(\frac{2 + (\gamma_{in} - 1)M_{tht}^2}{2 + (\gamma_{in} - 1)M_{in}^2} \right)^{\frac{\gamma_{in} + 1}{2(\gamma_{in} - 1)}}.$$
 (6)

The steady Mach number profile $\mathsf{M}_{\mathsf{tht}}(x)$ is extracted along the symmetry axis from the CFD simulation of the thermally choked flow and is used to compute the equivalent isentropic area distribution $\mathsf{A}_{\mathsf{is}}(x)$. Since the cross-section $\mathsf{A}_{\mathsf{is}}(x)$ is calculated assuming a constant heat capacity ratio $\gamma = \gamma_{\mathsf{in}}$, and further isentropic-flow calculations account for temperature variation, a small deviation arises between $\mathsf{M}_{\mathsf{is}}(x)$ and $\mathsf{M}_{\mathsf{tht}}(x)$. This has no impact on the conclusions.

2.5. Entropy-spot injection method

The entropy-spot injection is performed based on the Gibbs equation (eq. (4)). Linearizing eq. (4) using the perturbation convention $\chi(x,t) = \bar{\chi}(x) + \chi'(x,t)$, where $\bar{\chi}$ denotes the steady component and χ' the small perturbation of $\chi = [s,p,T]$, yields:

$$\frac{s'}{\bar{c}_p} = \frac{T'}{\bar{T}} - (\bar{\gamma} - 1)\frac{p'}{\bar{\gamma}\bar{p}},\tag{7}$$

Based on these considerations, the set of variables used to inject an entropy spot into the system are the static pressure and the static temperature.

At the inlet, the static pressure p is prescribed as constant ($p'_{\text{in}} = 0$). Consequently, a perturbation in the static temperature T' directly generates an entropy fluctuation s'. The inlet boundary conditions for the injection of a spot of radius R_s are thus defined as

$$p'_{\text{in}}/(\bar{\gamma}_{\text{in}}\bar{p}_{\text{in}}) = 0,$$
 (8) $T'_{\text{in}}/\bar{T}_{\text{in}} = \eta \left(1 + \cos(\pi r(t, y)/R_{\text{S}})\right)/2,$

where the instantaneous longitudinal center position is $x(t) = -x_0 + n \, \Delta x$, with x_0 the initial longitudinal position of the spot center and Δx the mesh size at the time step n, and $r(t,y) = \sqrt{x(t)^2 + (y-y_0)^2}$, where y_0 is the initial transverse position of the spot center. If the conditions $|x(t)| \leq R_{\rm s}$ and $|y-y_0| \leq \sqrt{R_{\rm s}^2 - x(t)^2}$ are not satisfied, then $T_{\rm in}'/\bar{T}_{\rm in} = 0$.

Once the entropy spot is fully generated, the inlet boundary condition is switched to a non-reflective boundary condition, allowing the evacuation of upstream-propagating acoustic waves generated by the convection of the entropy spot. This boundary condition acts as a low-frequency filter and is parametrized to have an inlet acoustic reflection coefficient of $R_{\rm in}=1\times10^{-4}$ for frequencies above $10\,{\rm Hz}$.

For this study, only half of an entropy spot is introduced into the nozzle after a delay of $\delta t=1\times 10^{-4}\,\mathrm{s}$ ($y_0=0$ and $x_0=R_\mathrm{s}+\bar{u}_\mathrm{in}\delta t$), unlike in the studies of Kowalski *et al.* [24] and Elbakly [25]. Thanks to the symmetry axis, this is equivalent to injecting a full circular entropy spot. In this study, the influence of the transverse injection position of the spot is not investigated. However, it is certainly a parameter that could affect the conclusions drawn below, since the amount of entropy injected into the flow depends on the fraction of the spot included in the domain.

3. One-dimensional entropy-noise models

To assess the impact of the thermal throat on the generation of acoustic noise due to the convection of entropy inhomogeneities, in comparison with a geometric throat nozzle, two one-dimensional models

are used. These models, proposed by Kowalski *et al.* [24] and Elbakly [25], determine whether the main sound generation mechanism is the quasi-steady response of the nozzle or inertial (acceleration) effects. The framework of these models applies to isentropic geometric nozzles and characterizes the asymptotic size limits of entropy spots relative to the throat height, $R_{\rm s}/y_{*}$, where $R_{\rm s}$ is the spot radius and y_{*} the nozzle height at the critical throat location (see fig. 2). The critical nozzle height is assumed to play a role in entropy-noise generation. For very large spots, the quasi-steady limit is approached, whereas for very small spots, the inertial limit is reached.

3.1. Quasi-steady asymptotic limit model

For a very large entropy spot, *i.e.*, $R_{\rm s}/y_*\gg 1$, the spot can be approximated as a one-dimensional entropy wave. Based on this consideration, the quasi-steady (QSS) model of Marble and Candel [26] can be applied. This model relies on two assumptions. First, in the quasi-steady limit, the critical throat Mach number fluctuations vanish under entropy wave forcing, *i.e.*, $M_*'=0$. Second, the nozzle is assumed to be compact, meaning that the acoustic wavelength λ is much greater than the nozzle length. Under the compact assumption, the relation $M_*'=0$ holds at any position within the subsonic region, and in particular at the inlet, where $M_{\rm in}'=0$. By expressing the Mach number fluctuations in terms of the natural variables p' and s', one obtains the inlet relation:

$$|p'_{\mathsf{in}}| = \frac{\bar{\gamma}_{\mathsf{in}}\bar{p}_{\mathsf{in}}\bar{\mathsf{M}}_{\mathsf{in}}}{2 + (\bar{\gamma}_{\mathsf{in}} - 1)\bar{\mathsf{M}}_{\mathsf{in}}} \frac{|s'_{\mathsf{in}}|}{\bar{c}_{p,\mathsf{in}}},\tag{9}$$

which describes the ratio between the maximum upstream-propagating acoustic wave amplitude $|p'_{in}|$ and the maximum downstream-propagating entropy wave amplitude $|s'_{in}|$.

Recent studies [21, 23] have shown that, for a thermal throat configuration, the quasi-steady condition $M_{*}'=0$ at the critical throat is never strictly valid, and that its value depends on the amount of added energy. Furthermore, the compact assumption cannot be applied due to the presence of heat addition. For clarity, the QSS model is nonetheless used here to compare both nozzle configurations.

It is noteworthy that this model assumes a uniform distribution of acoustic and entropic fluctuations across the transverse direction, which holds for very large spots but becomes questionable for smaller spot sizes.

3.2. Point-mass inertial asymptotic limit model

For a very small entropy spot, i.e., $R_{\rm s}/y_*\ll 1$, the spot can be approximated as a point sound source of excess mass density m_e that generates the acoustic response at a given source position x_s . Following the work of Elbakly [25], the upstream acoustic response $|p'_{\rm in}|$ due to a point excess mass density m_e at position x_s is given by:

$$|p_{\mathsf{in}}'| = \sqrt{\frac{\bar{\rho}_{\mathsf{in}}\bar{c}_{\mathsf{in}}}{\bar{\rho}_{s}\bar{c}_{s}}} \frac{1}{\mathsf{A}_{\mathsf{in}}\mathsf{A}_{s}} \left[(1 + \bar{\mathsf{M}}_{s}) - R(1 - \bar{\mathsf{M}}_{s}) \right] \left(\frac{1 - \bar{\mathsf{M}}_{s}}{1 - \bar{\mathsf{M}}_{\mathsf{in}}} \right) \bar{u}_{s} \left. \frac{\mathsf{d}\bar{u}}{\mathsf{d}x} \right|_{s} \frac{m_{e}}{2}, \tag{10}$$

where R is the quasi-steady acoustic reflection coefficient derived by Marble and Candel [26]:

$$R = \frac{2 - (\bar{\gamma}_s - 1)\bar{\mathsf{M}}_s}{2 + (\bar{\gamma}_s - 1)\bar{\mathsf{M}}_s}.$$
 (11)

The point-mass (PM) model assumes that, for sufficiently small entropy spots, acoustic generation is solely due to inertial effects, and that the acoustic response scales with the excess mass m_e contained in the spot.

To estimate the sound source position x_s , the methodology of Elbakly [25] is used. The position at which the quantity $|p_{\rm in}'|{\sf A}_{\rm in}^3/(m_e\bar{u}_{\rm in}^2)$ reaches its maximum is taken as the location where the maximum acoustic sound is generated.

The excess mass density m_e is then numerically estimated by volumetric integration in a volume $\mathcal V$ of the density fluctuations $\rho_e'=(\rho-\bar\rho)/\bar\rho$ over the constant-duct region, so that $m_e=\int_{\mathcal V}\rho_e'\mathrm{d}\mathcal V$. This numerical

integration is performed at a fixed longitudinal position $x_{\rm sensor}$ over the total simulation time $\tau_{\rm CFD}$ and across the transverse height y of the duct. It has been verified that this method is not sensitive to the sensor position within the constant duct. Further details on the point-mass model are provided in the work of Elbakly [25]. It should be noted that this model is based on the isentropic nozzle assumption, which is not valid for the thermal throat configuration. Nevertheless, it provides valuable insight into the sound-generation mechanisms for both choked configurations considered.

4. Numerical set-up

The numerical simulations are performed using the ONERA unstructured CFD code CEDRE [37], which solves the Euler equations (eq. (1)).

The computational setup consists of a two-dimensional planar domain, as described in section 2.1, discretized with $950\,000$ computational cells of size $\Delta x/L = 1\times 10^{-4}$ (see fig. 2). This resolution ensures adequate spatial discretization of the entropy spot, providing at least 40 points per spot radius for the smallest size considered ($R_{\rm s}/y_*=1$). Since the flow is primarily longitudinal, the same grid spacing ($\Delta x \simeq \Delta y$) is applied in both directions, resulting in approximately 9500 points along the longitudinal axis and 100 points along the transverse axis. Spatial discretization employs a second-order multi-slope MUSCL scheme [38] combined with an HLLC flux scheme [39].

Temporal integration is carried out using an implicit second-order Runge-Kutta scheme [40] with a time step $\Delta t = 2.5 \times 10^{-7}\,\mathrm{s}$, corresponding to a Courant-Friedrichs-Lewy (CFL) number of $\bar{u}_{\rm in}\,\Delta t/\Delta x = 0.28$. The unsteady solutions, described in section 2.5, are post-processed using a time step modulated according to the circular spot radius. To allow the convection of a fully developed entropy spot through the nozzle geometry and to measure the maximum acoustic response, the simulation time is set to $\tau_{\rm CFD} = 30\,R_{\rm s}/\bar{u}_{\rm in}$. For adequate temporal resolution, $1000\,\mathrm{time}$ steps are saved per run. For the geometric-throat configuration (see section 2.4), the same numerical parameters are used, ensuring mesh and time-step independence.

The sensitivity of the acoustic results to the mesh and time-step resolution was assessed by refining the discretization to $\Delta x/L = 5 \times 10^{-5}$ and $\Delta t = 1 \times 10^{-7}$ s for a spot size of $R_{\rm s}/y_* = 1$. The relative difference in the upstream-propagating acoustic wave remained below 4×10^{-3} .

5. Discussion and results

5.1. Steady base flow-fields

Once the steady state is reached, the steady flow fields (Mach number $\bar{\rm M}$, static pressure \bar{p} , and static temperature \bar{T}) are obtained from the two-dimensional CFD simulation. The maximum amplitude of the entropy spot (at its center) is fixed at $\eta=1\times 10^{-2}$ to ensure a linear acoustic response, as verified for a geometric nozzle by Olivon *et al.* [21].

Figure 3 shows the two-dimensional steady Mach number $\bar{\rm M}$ for the two nozzle geometries considered. For the thermally choked flow configuration, the thermal throat is located at a reduced length of $x_*/L=0.8$, as expected. Owing to the non-uniform volumetric heat source term P_v , the Mach number increases continuously along the divergent duct. For the geometric throat case, the throat is positioned at the same location, as determined from eq. (6). A deviation of up to 5×10^{-4} in the steady Mach number field is observed between the geometric and thermal throat cases, which has no impact on the following conclusions. This deviation arises because the heat capacity ratio γ is assumed constant in the geometric throat calculation of eq. (6) (fixed to the inlet value of the thermal-throat case, $\gamma_{\rm tht,in}=1.379$), whereas in the CFD simulation it varies from $\gamma_{\rm geo,in}=\gamma_{\rm tht,in}=1.379$ at the inlet to $\gamma_{\rm geo,*}=1.397$ at the throat.

Figure 4 shows the steady static pressure \bar{p} and temperature \bar{T} as a function of the longitudinal length x/L. The quantities are obtained from the CFD simulations and are extracted along the symmetry axis. As expected, as the velocity is increasing, the static pressure is decreasing for both configurations. However, for the thermal throat choking configuration, as energy is added to the flow, the static temperature is increasing from $T_{\rm in}=560\,{\rm K}$ at the inlet to $T_*\approx1740\,{\rm K}$ at the throat position. This substantive temperature elevation induces a variation of the heat capacity ratio from $\gamma_{\rm tht,in}=1.379$ to $\gamma_{\rm tht,*}=1.304$.

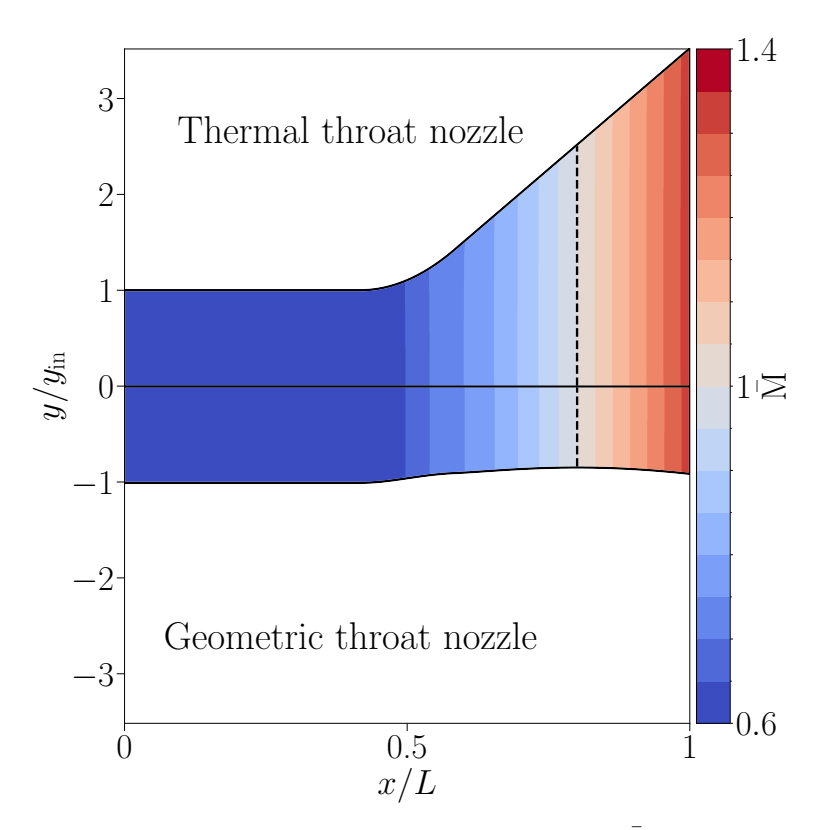


Fig 3. (Colour online) Two-dimensional steady-state Mach number, \overline{M} , for the thermal (top) and geometric throat (bottom) choking cases obtained with the CFD solver. The sonic line is shown (- - -).

5.2. Entropy-spot size asymptotic behavior

A series of entropy spot injections is performed for both the thermal and geometric throat configurations, with spot radii ranging from $R_{\rm s}/y_*=1$ to 500. This wide range of spot sizes provides a representation of the main mechanisms occurring in both choking configurations.

Figure 5 presents the maximum acoustic response obtained from the CFD simulations, normalized either by the point-mass inertial model (eq. (10), $|p'_{\text{max}}|_{\text{CFD}}/|p'_{\text{max}}|_{\text{PM}}$) or by the QSS model (eq. (9), $|p'_{\text{max}}|_{\text{CFD}}/|p'_{\text{max}}|_{\text{QSS}}$), for the convection of an entropy spot through either a thermal or a geometric throat, as in the work of Elbakly [25]. This representation directly indicates whether the dominant mechanism of entropy-noise generation is inertial ($|p'_{\text{max}}|_{\text{CFD}}/|p'_{\text{max}}|_{\text{PM}} \rightarrow 1$) or quasi-steady ($|p'_{\text{max}}|_{\text{CFD}}/|p'_{\text{max}}|_{\text{QSS}} \rightarrow 1$).

For the geometric throat, the asymptotic behavior is in good agreement with both the point-mass model (\blacksquare) and the quasi-steady model (\square). At very small spot radii, the acoustic response approaches an asymptotic value of about 1.05, which is very close to the pure inertial prediction. The inertial regime is reached for relatively large spot sizes, $R_{\rm s}/y_* < 10$, which is noteworthy in the context of ramjet-base geometries. For very large spots, the QSS acoustic response is reached for $R_{\rm s}/y_* > 200$, with an asymptotic value of approximately 0.97. Between these two asymptotic limits lies a transition region where neither the point-mass nor the QSS mechanism dominates.

For the thermally choked-flow configuration, despite the steady component evolution of the Mach number being similar to that of the geometric throat, the acoustic response differs markedly. For very large spots, the QSS regime is reached for smaller spot sizes, around $R_{\rm S}/y_*>40$ (°). As expected, the ratio $|p'_{\rm max}|_{\rm QSS}$ is greater than unity (close to 1.25), which is consistent with observations in similar thermally choked flow configurations [21, 22]. This is because the QSS model assumes $M'_*=0$ at the throat, which is invalid for a heated nozzle geometry. Physically, this means that the acoustic waves

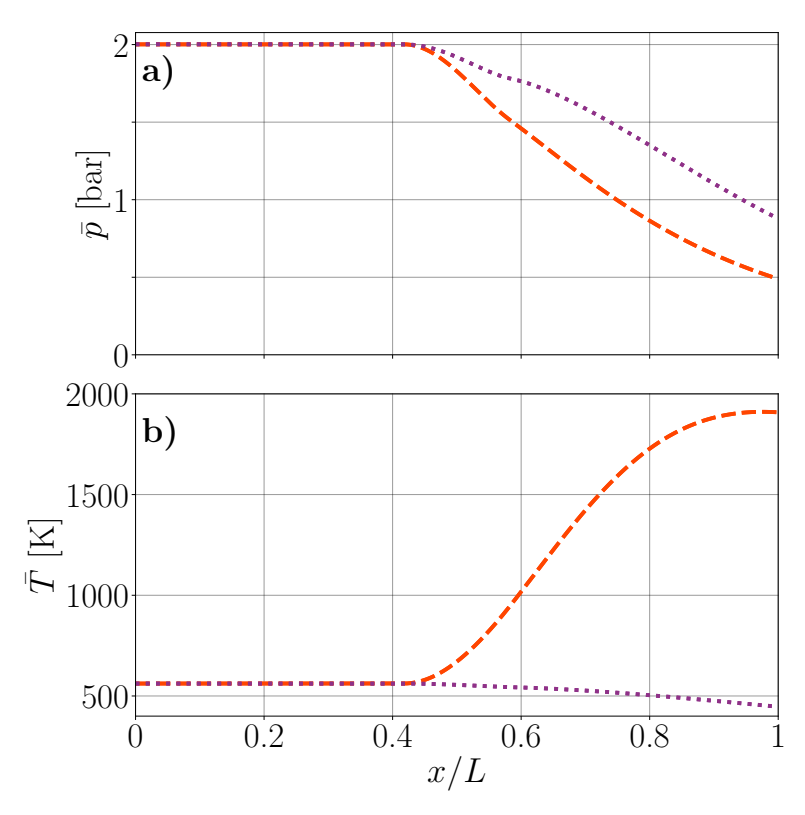


Fig 4. (Color online) Steady-state flow fields as a function of the longitudinal length x/L for the geometric (\cdots) and thermal throat (---) choking cases obtained from CFD results. The static pressure $(\bar{p}, (a))$ and the static temperature $(\bar{T}, (b))$ are displayed.

generated within the heated region are accompanied by an additional entropy response, which superposes with the initial upstream-propagating acoustic waves, leading to an amplified overall response. For very small spots, the inertial regime (•) appears to be reached for $R_{\rm s}/y_{*} < 2$, although with a value different from unity (≈ 0.65). This damping effect remains unexplained.

In all cases, both the thermal- and geometric-throat nozzles exhibit similar asymptotic acoustic response mechanisms in the large- and small-spot-size limits, though at different dimensionless spot sizes.

6. Conclusions

Indirect entropy noise generated within thermally choked flow by a two-dimensional circular entropy spot has been numerically and analytical investigated. Two configurations were examined: one with a thermal throat and one with an isentropic geometric throat. Both nozzle geometries were designed to have the same steady Mach number distribution, enabling a direct comparison of their acoustic responses. To analyze asymptotic behavior with respect to spot size, two reference models were considered: the quasisteady (QSS) model for very large spots, and the point-mass (PM) model for very small spots.

The results show that, for very large spots, both nozzle configurations tend toward a quasi-steady response, but at different spot sizes. The thermal throat configuration reaches this regime at a smaller spot size than the geometric-throat case. Furthermore, owing to its underlying assumptions, the QSS model correctly predicts the asymptotic trend but not the exact amplitude of the response. The acoustic response of the thermal-throat configuration is higher, due to the influence of the heated region.

For very small spots, the point-mass model predicts the inertial noise mechanism with reasonable accuracy, indicating that inertial effects dominate sound generation in this regime. However, for the thermal-throat configuration, the CFD results deviate from the model at the smallest spot sizes, yielding an

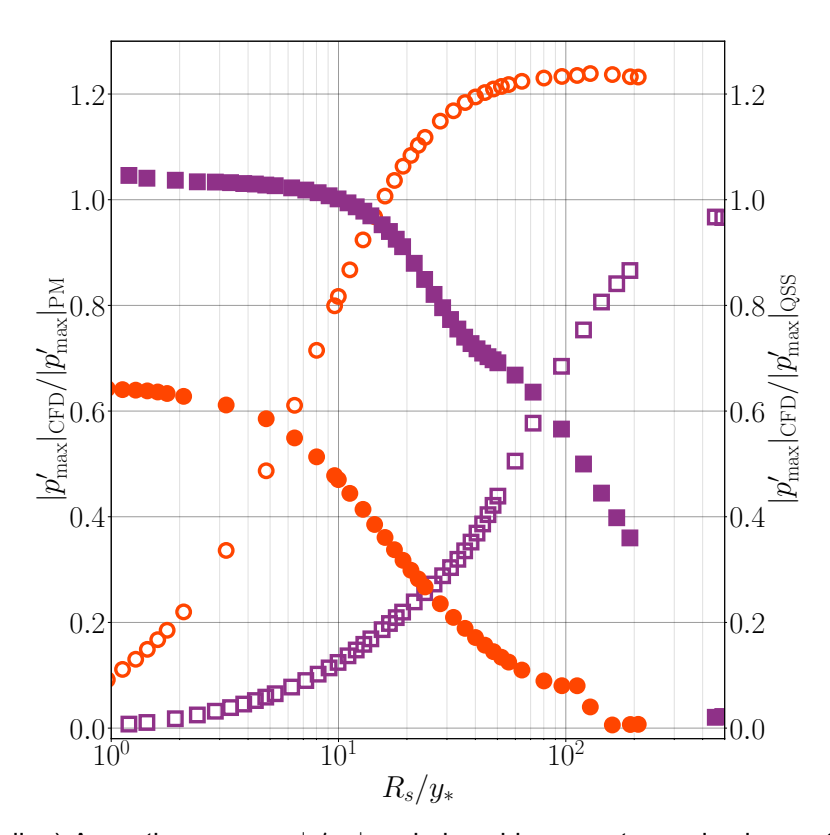


Fig 5. (Color online) Acoustic response $|p'_{\text{max}}|_{\text{CFD}}$ induced by an entropy circular spot. The response is normalized on the left by the point-mass model $|p'_{\text{max}}|_{\text{PM}}$ (eq. (10), full markers) and on the right by the QSS model $|p'_{\text{max}}|_{\text{QSS}}$ (eq. (9), empty markers). Results are shown for the thermally choked flow configuration (\bullet , \circ) and the geometric throat case (\bullet , \Box).

acoustic response lower than that predicted by the point-mass model. The mechanism responsible for this acoustic response damping has not yet been identified.

To extend this study, it is important to adapt the QSS and PM models to non-isentropic heated base flows in order to better capture the asymptotic mechanisms in thermal-throat configurations. Moreover, the range of spot radii should be extended to match more realistic conditions, particularly at very small spot scales. In addition, this work has been carried out under the assumption of a linear acoustic response; the validity range of this approximation should be assessed for the considered cases. Finally, the influence of the entropy-spot shape, the transverse and longitudinal injection positions, and the spatial distribution of heat addition should be investigated to cover a wider range of nozzle geometries.

Acknowledgments

F.O. and A.G. thank E. Bekaert for the discussions on the ramjet-based numerical simulations. F.O. and A.G. thank A. Hirschberg, L. Hirschberg, and K. Elbakly for the insightful discussions. A.G. thanks F. Méry, A. Boucher, P. Villedieu, O. Dessornes and J. Anthoine for their support.

A. Quasi-one-dimensional steady-state volumetric power models

To establish a thermal throat deep within a divergent nozzle, a steady-state quasi-one-dimensional non-uniform volumetric heat-release rate $P_v(x)$ must be defined. To correctly tune this source term, an analytical steady-state quasi-one-dimensional model for a calorically semi-perfect ideal-gas flow, developed in [30, 32, 33], is employed. It is based on the instantaneous heat addition q, which, in the

quasi-one-dimensional approximation, is related to the volumetric power through

$$P_v = \rho u \frac{\mathrm{d}q}{\mathrm{d}x}.\tag{12}$$

The principle of the model is as follows: for a prescribed steady-state thermal-throat position x_* , an initial guess of the Damköhler number D_1 is made, and the Mach-number evolution $\mathbf{M}(x)$ is computed from the sonic position back to the inlet. The computed inlet Mach number is then compared with the prescribed boundary value \mathbf{M}_{in} . If both match, the corresponding volumetric power profile is determined and used in the CFD solver. Otherwise, D_1 is updated, and the procedure is repeated until convergence, using a Newton–Raphson algorithm. The initial guess of D_1 is typically of order unity.

The shape of the energy-release profile follows Wang et al. [34]:

$$q(x,\sigma) = \frac{D_1}{c_{p,\text{in}}T_{0,\text{in}}} \frac{1 - \exp\left(-\left(\frac{x - x_{\text{u}}}{\sigma}\right)^2\right)}{1 - \exp\left(-\left(\frac{L - x_{\text{u}}}{\sigma}\right)^2\right)},\tag{13}$$

where D_1 is the Damköhler number, $T_{0,\text{in}}$ is the inlet total temperature, $c_{p,\text{in}}$ is the inlet isobaric heat capacity, x is the longitudinal coordinate, x_{u} is the start of the energy-release region, L is the total nozzle length, and σ is the characteristic width of the energy-release zone.

It is noteworthy that the width of the energy-release region, σ , is directly related to the cross-sectional area at the sonic location through the critical-throat relation of [36]:

$$\frac{\mathsf{dA}}{\mathsf{A}}\bigg|_{x_0} = \frac{\mathsf{d}q}{c_p T}\bigg|_{x_0}.\tag{14}$$

The static temperature at the sonic position is obtained from the conservation of total specific enthalpy:

$$h_{0,\text{in}} + q(x) = h(x) + \frac{\gamma r T(x) \mathsf{M}^2(x)}{2},$$
 (15)

where the specific enthalpy h(x) is evaluated from:

$$h(x) = \int_{T_{\text{ref}}}^{T(x)} c_p(T) \, \mathrm{d}T, \tag{16}$$

with $r = \mathcal{R}/\mathcal{W}$ the specific gas constant, \mathcal{R} the universal gas constant, and \mathcal{W} the molar mass of the gas.

The quasi-one-dimensional, steady-flow evolution of a calorically semi-perfect ideal gas is described by the following three governing equations [35]:

$$\frac{\text{dM}}{\text{M}} = -\frac{1 + \frac{\gamma - 1}{2} \text{M}^2}{1 - \text{M}^2} \frac{\text{dA}}{\text{A}} + \frac{1 + \gamma \text{M}^2}{1 - \text{M}^2} \frac{\text{d}q}{2c_p T} - \frac{\text{d}\gamma}{2\gamma}, \tag{17}$$

$$\frac{dT}{T} = \frac{(\gamma - 1)M^2}{1 - M^2} \frac{dA}{A} + \frac{1 - \gamma M^2}{1 - M^2} \frac{dq}{c_p T},$$
(18)

$$c_p = \sum_{n=0}^{7} \frac{\alpha_n}{\mathcal{W}} T^n \quad \text{[29]}.$$

For a given steady-state thermal-throat position x_* and an initial guess of the Damköhler number D_1 , the width σ of the energy-release profile $q(x,\sigma)$ is computed using eqs. (14) and (15). The Mach number M(x) and static temperature T(x) profiles are then obtained by iteratively solving eqs. (17) and (18) with a first-order backward discretization scheme. The heat capacity ratio γ at each position is evaluated from eq. (19) using the local static temperature T.

References

- [1] F. Falempin. Ramjet and dual mode operation. Technical Report RTP-EN-AVT-150, NATO, 2008.
- [2] O. Dessornes and D. Scherrer. Tests of the JAPHAR dual-mode ramjet engine. *Aerosp. Sci. Technol.*, 9(3):211–221, 2005.
- [3] W. Li, D. Zhao, X. Chen, Y. Sun, Siliang Ni, Di Guan, and Bing Wang. Numerical investigations on solid-fueled ramjet inlet thermodynamic properties effects on generating self-sustained combustion instability. *Aerosp. Sci. Technol.*, 119:107097, 2021.
- [4] J. E. Crump, K. C. Schadow, V. Yang, and F. E. C. Culick. Longitudinal combustion instabilities in ramjet engines: Identification of acoustic modes. *J. Propul. Power*, 2(2):105–109, 1986.
- [5] V. Yang and F. E. C. Culick. Analysis of low-frequency combustion instabilities in a laboratory ramjet combustor. *Combust. Sci. Technol.*, 45(1–2):1–25, 1986.
- [6] E. George, V. Sabelnikov, and P. Marge. Self-ignition of ethylene/hydrogen mixtures in unsteady thermal choking conditions: Numerical unsteady RANS investigation. In *Proceedings of the West-East High Speed Flow Field Conference*, pages 1–12, Moscow, 2007.
- [7] A. Roux, L. Y. M. Gicquel, Y. Sommerer, and T. J. Poinsot. Large-eddy simulation of mean and oscillating flow in a side-dump ramjet combustor. *Combust. Flame*, 152(1–2):154–176, 2008.
- [8] J.-M. Klein, A. Genot, A. Vincent-Randonnier, and A. Mura. Combustion thermoacoustics: On the relevance of some stability criteria. In *EUCASS-3AF*, pages 1–15, 2022.
- [9] E. Bekaert, A. Genot, T. Le Pichon, and T. Schuller. Longitudinal acoustic field in a two-phase ramjet: Numerical simulation and acoustic models. In *HiSST: 3rd International Conference on High-Speed Vehicle Science Technology*, page 151, 2024.
- [10] S. Boulal, A. Genot, J.-M. Klein, Y. Fabignon, A. Vincent-Randonnier, and V. Sabelnikov. On the hydro-acoustic coupling responsible for the flashback limit-cycle of a premixed flame at a backward-facing step. *Combust. Flame*, 257:112999, 2023.
- [11] A. S. Morgans and D. Yang. Thermoacoustic instability in combustors. Annu. Rev. Fluid Mech., 2024.
- [12] N. Karimi, M. J. Brear, and W. H. Moase. Acoustic and disturbance energy analysis of a flow with heat communication. J. Fluid Mech., 597:67–89, 2008.
- [13] S. R. Yeddula, R. Gaudron, and A. S. Morgans. Acoustic absorption and generation in ducts of smoothly varying area sustaining a mean flow and a mean temperature gradient. *J. Sound Vib.*, 515:116437, 2021.
- [14] N. Karimi, M. J. Brear, and W. H. Moase. On the interaction of sound with steady heat communicating flows. *J. Sound Vib.*, 329(22):4705–4718, 2010.
- [15] A. Giauque, M. Huet, and F. Clero. Analytical analysis of indirect combustion noise in subcritical nozzles. *J. Eng. Gas Turbines Power*, 134(11):111202, 2012.
- [16] J. Nan, J. Li, A. S. Morgans, L. Qin, and L. Yang. Theoretical analysis of sound propagation and entropy generation across a distributed steady heat source. *J. Sound Vib.*, 536:117170, 2022.
- [17] V. K. Rani and S. L. Rani. WKB solutions to the quasi one-dimensional acoustic wave equation in ducts with non-uniform cross-section and inhomogeneous mean flow properties: Acoustic field and combustion instability. *J. Sound Vib.*, 436:183–219, 2018.
- [18] S. Basu and S. L. Rani. Generalized acoustic Helmholtz equation and its boundary conditions in a quasi one-dimensional duct with arbitrary mean properties and mean flow. *J. Sound Vib.*, 512:116377, 2021.
- [19] S. R. Yeddula, J. Guzmán-Iñigo, and A. S. Morgans. A solution for the quasi-one-dimensional linearised Euler equations with heat transfer. *J. Fluid Mech.*, 936:R3, 2022.
- [20] A. Jain and L. Magri. A physical model for indirect noise in non-isentropic nozzles: transfer functions and stability. J. Fluid Mech., 935, 2022.
- [21] F. Olivon, A. Genot, J.-E. Durand, A. Hirschberg, and E. Piot. On the linear aeroacoustic response of a thermally choked nozzle to acoustic and entropy plane waves. *J. Sound Vib.*, 2025. submitted.

- [22] F. Olivon, A. Genot, J.-E. Durand, A. Hirschberg, and E. Piot. A quasi-one-dimensional critical-throat acoustic boundary condition for thermally choked dual-mode ramjet nozzles. *Acta Acust. united Ac.*, 2025. submitted.
- [23] F. Olivon, A. Genot, L. Hirschberg, S. Moreau, and A. Hirschberg. On critical-throat boundary condition in quasi-one-dimensional linearized Euler equations models. *J. Fluid Mech.*, 2025. in press.
- [24] K. Kowalski, S. J. Hulshoff, P. Ströer, J. Withag, A. Genot, A. S. Morgans, F. Bake, K. Venner, M. Sanders, and L. Hirschberg. Entropy-patch–choked-nozzle interaction: Quasi-steady modeling-regime limits probed. In 30th AIAA/CEAS Aeroacoustics Conference (2024), pages 1–24, Rome, Italy, 2024. American Institute of Aeronautics and Astronautics.
- [25] K. Elbakly. Entropy-patch choked-nozzle interaction: Inertial, quasi-steady, linear, and non-linear modeling regimes mapped. Master's thesis, University of Twente, 2025.
- [26] F. E. Marble and S. M. Candel. Acoustic disturbance from gas non-uniformities convected through a nozzle. *J. Sound Vib.*, 55(2):225–243, 1977.
- [27] I. Durán and S. Moreau. Solution of the quasi-one-dimensional linearized Euler equations using flow invariants and the Magnus expansion. *J. Fluid Mech.*, 723:190–231, 2013.
- [28] M. Huet, A. Emmanuelli, and T. Le Garrec. Entropy noise modelling in two-dimensional choked nozzle flows. *J. Sound Vib.*, 488:115637, 2020.
- [29] E. W. Lemmon, R. T. Jacobsen, S. G. Penoncello, and D. G. Friend. Thermodynamic properties of air and mixtures of nitrogen, argon, and oxygen from 60 to 2000 K at pressures to 2000 MPa. *J. Phys. Chem. Ref. Data*, 29(3):331–385, 2000.
- [30] J.-E. Durand and F. Olivon. Thermally choked nozzle flow 1D model for low-Mach dual-mode scramjet performance assessment. In 3rd International Conference on High-Speed Vehicle Science & Technology, page 130, 2024.
- [31] S. R. Yeddula, J. G. Guzmán Iñigo, and A. Morgans. Effect of steady and fluctuating heat transfer on acoustic and entropy transfer functions of a nozzle. In *28th AIAA/CEAS Aeroacoustics Conference*, pages 1–12, Southampton, UK, 2022. American Institute of Aeronautics and Astronautics.
- [32] F. Olivon, J.-E. Durand, A. Genot, and E. Piot. Unsteady forced motion of the thermal throat in a low-Mach dual-mode ramjet nozzle. In *EUCASS-3AF*, page 558, Lausanne, 2023.
- [33] F. Olivon, J.-E. Durand, A. Genot, and E. Piot. High-frequency acoustic propagation in a thermally choked low-Mach dual-mode ramjet. In 30th AIAA/CEAS Aeroacoustics Conference (2024), pages 1–15, Rome, Italy, 2024. American Institute of Aeronautics and Astronautics.
- [34] H. Wang, Q. Yang, and X. Xu. Effect of thermal choking on ejection process in a rocket-based combined cycle engine. Appl. Therm. Eng., 116:197–204, 2017.
- [35] A. H. Shapiro. *The Dynamics and Thermodynamics of Compressible Fluid Flow. Vol. 1*. Wiley, New York, 23rd printing edition, 1976.
- [36] W. H. Heiser and D. T. Pratt. Hypersonic Airbreathing Propulsion. AIAA, Washington, D.C., 1994.
- [37] A. Refloch, B. Courbet, A. Murrone, P. Villedieu, C. Laurent, P. Gilbank, J. Troyes, L. Tessé, G. Chaineray, J.-B. Dargaud, E. Quémerais, and F. Vuillot. Cedre software. *AerospaceLab J.*, 2011.
- [38] C. Le Touze, A. Murrone, and H. Guillard. Multislope MUSCL method for general unstructured meshes. *J. Comp. Phys.*, 284:389–418, 2015.
- [39] E. F. Toro, M. Spruce, and W. Speares. Restoration of the contact surface in the HLLC riemann solver. *Shock Waves*, 4(1):25–34, 1994.
- [40] J. C. Butcher. Implicit Runge-Kutta processes. Math. Comp., 18(85):50-64, 1964.